First search for an anomalous excess of charged-current ν_e interactions without visible pions using the full MicroBooNE dataset

The MicroBooNE Collaboration*
(Dated: June 12, 2024)

This public note presents an investigation of low-energy electron-neutrino events in the Fermilab Booster Neutrino Beam by the MicroBooNE experiment. This search is motivated by the excess of low energy electromagnetic events observed by the MiniBooNE experiment and, more broadly, by the landscape of neutrino anomalies observed at short baselines. This is the first measurement to use all of the data collected by the MicroBooNE experiment, corresponding to 1.1×10^{21} protons on target. Two exclusive samples of electron neutrinos without visible pions are used, one with visible protons and one without any visible protons. MicroBooNE data is compared to two empirical models of the MiniBooNE low energy excess, one obtained by enhancing the electron-neutrino content as a function of the neutrino energy, and one representing the excess for the first time as a function of the kinematics of shower energy and angle. This measurement excludes an electron-like interpretation of the MiniBooNE excess based on these models at $\geq 99\%$ confidence level in all kinematic variables.

I. INTRODUCTION

One of the primary goals of the MicrobooNE experiment [1] is to explore the nature of the low energy excess (LEE) of electromagnetic activity observed by the MiniBooNE experiment [2]. A first set of measurements using the first three years of MicroBooNE data explored the possibility of an excess due to an electron neutrino enhancement in multiple topologies [3–6], as well as one caused by an excess of neutral current Δ radiative decays [7]. This analysis builds on [3] and uses the entirety of the MicroBooNE data sets to measure the rate of charged current (CC) electron neutrino interactions without detected pions in the final state. Relative to [3], the analysis philosophy is unchanged: this update keeps the same signal definition, the same version of the GENIE generator [8] as baseline Monte Carlo (MC), the same Pandora event reconstruction [9] chain, and considers the same set of systematic uncertainties. Major upgrades to the result include the use of the full Micro-BooNE data set of 1.1×10^{21} protons on target (POT) for the first time, a new model for the MiniBooNE signal using visible shower energy and angle kinematics, the use of additional constraint samples, and the use of the cosmic ray tagger (CRT) subdetector [10] in the selections.

The note is organized as follows. In Section II, we provide a description of the selections, including the expanded set of constraint channels, followed by an overview of the uncertainty treatment in Section III. We then describe a new model for the LEE in Section IV. Finally, we present a comparison of data to models and the associated statistical tests in Section V.

* microboone_info@fnal.gov

II. EVENT SELECTION AND SIDEBANDS

The selection strategy in this measurement is mostly unchanged from Ref. [3]. The analysis selects electron neutrino events without visible pions, corresponding to the electron neutrino signal definition in MiniBooNE [2]. We consider two signal channels: The $1e0p0\pi$ channel selects events with no visible protons, and the $1eNp0\pi$ channel selects events with visible protons (proton energy above 40 MeV). The presence of a proton at the vertex for $1eNp0\pi$ events enhances the selection efficiency and reduces the background of this channel compared to the the $1e0p0\pi$ channel. Both the $1e0p0\pi$ and $1eNp0\pi$ selections were not changed from those presented in Ref. [3], except for the addition of new CRT-based cuts to boost the background rejection in the $1e0p0\pi$ channel. When used as a standalone tool, the CRT removes 60% of the cosmic ray background while rejecting only 3% of the ν_e interactions, as shown in Appendix A. In its application to this analysis, the CRT rejection power is somewhat reduced because the dataset analyzed includes data from runs 1 and 2 (when the CRT subsystem was not installed) and the original background rejection strategy had to be optimized based on TPC morphology variables only. Still, when added to the $1e0p0\pi$ selection, CRT-based cuts reject an additional 25.4% of the remaining cosmic ray background, with a 98.9% efficiency for the electron neutrinos. Both signal channels are dominated by charged current electron neutrinos, with neutral current (NC) interactions containing final-state π^0 mesons constituting the dominant background, particularly in the $1e0p0\pi$ channel.

This analysis uses sidebands to constrain the prediction of the selected MC events for both the $1eNp0\pi$ and $1e0p0\pi$ channels, and to reduce the associated systematic uncertainty in a data-driven way. Two sidebands target charged current ν_μ interactions in the absence of pions: $1\mu0p0\pi$ and $1\mu Np0\pi$, matching the final state hadronic

observables of the electron neutrino samples. The high-statistics muon neutrino channels constrain the intrinsic electron neutrino predictions, leveraging strong correlations in cross-section (through assumed lepton universality), flux (through their shared parentage from pions and kaons), and detector uncertainties. A third sideband constrains the largest source of background neutrino interactions in the $1e0p0\pi$ signal channel: mis-reconstructed neutral pions. The selection for this sideband identifies events with at least two showers and no visible tracks (protons, muons, pions) to enhance the number of NC interactions containing π^0 mesons (referred to as ν NC π^0 events). This requirement is orthogonal to the electron neutrino selection, which requires exactly one shower to limit the amount from π^0 mesons.

The distribution of the observed events in the three sideband channels is shown in Fig. 1. All three channels show reasonable agreement between data and simulation, suggesting adequate modeling of these processes. For these sidebands we use data collected during periods when information from the CRT was available, corresponding to 6.38×10^{20} POT (an increase in side band data of 3× over [3]).

The conditional constraint formalism described in Ref. [3] uses the three sidebands to constrain the models of the two signal channels. The full covariance matrix utilized in this analysis is reported in Appendix B.

This is the first analysis to incorporate the full MicroBooNE dataset which was taken over a span of five years. Data-MC agreement for the variables employed in the event selections was cross checked to validate the stability of the analysis across run periods. The validation work confirmed that the detector response remained stable across runs, with findings consistent with our published analysis [3].

III. UNCERTAINTY TREATMENT

The set of systematic uncertainties applied in this analysis is unchanged from that of Ref. [3]; a brief overview is given here. Four categories are included: neutrino flux, neutrino interaction cross sections, secondary interactions of hadrons outside of the target nucleus, and the detector response model. The covariance matrices for each of these sources of uncertainties are calculated including the correlations between all signal and sideband channels and added together. The resulting full covariance matrix is shown in Appendix B.

In the case of the flux, cross section, and secondary interaction uncertainties, variations from the central value are obtained through a reweighting procedure, while for the detector response uncertainties the covariance is obtained by propagating a set of simulated neutrino interactions through several detector models [11]. As an update to the earlier iteration of this analysis, correlations in detector systematics across bins and across different channels are fully accounted for with the use of a smoothing
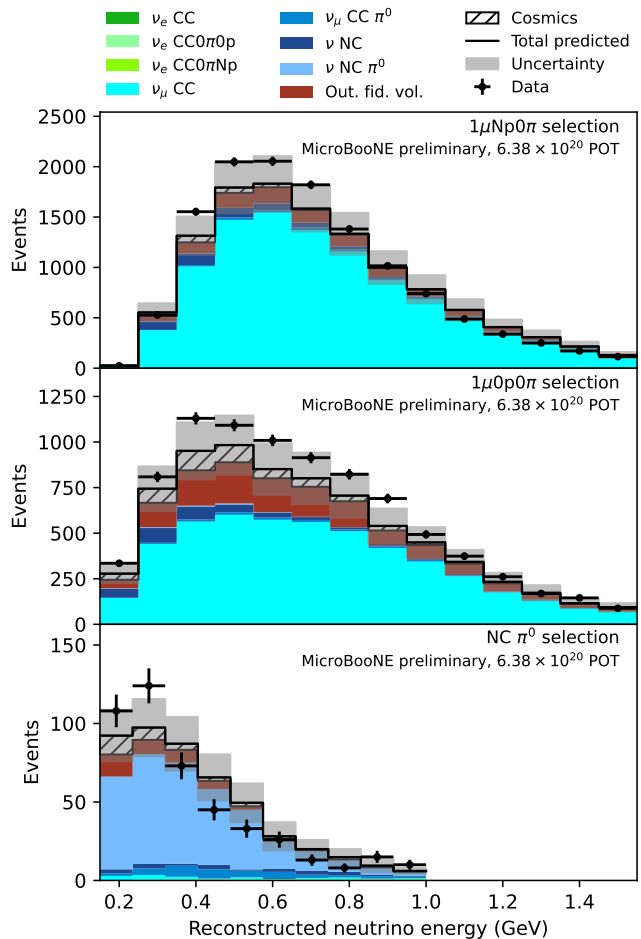

FIG. 1. The sideband selected data events compared with the prediction. The prediction is broken down into charged-current (CC) ν_e and ν_μ interactions, neutral-current (NC) interactions, neutral pion producing interactions, neutrino interactions outside of the fiducial volume, and cosmic rays mistaken for neutrino interactions. The CC ν_e interactions are further subdivided into those producing no protons or pions (ν_e CC 0π0p), those producing some protons and no pions (ν_e CC 0πNp) and all other ν_e interactions (ν_e CC). The NC π^0 selection only includes events up to 1 GeV due to low statistics above this energy.

algorithm to minimize the impact of statistical fluctuations in detector variation sample statistics.

The statistical uncertainty due to Poisson fluctuations of the data is incorporated into the analysis by adding a combined Neyman-Pearson (CNP) covariance matrix [12] to the total covariance that is used to calculate the χ^2 between the predicted and observed bin counts.

As with the previous result [3], we use the block matrix method [13, p. 116–117] to constrain the prediction in the $1e0p0\pi$ and $1eNp0\pi$ signal channels channels using the data in the ν_μ and π^0 sideband channels. The impact of these constraints on the predicted event rate and systematic uncertainty is illustrated in Appendix B.

IV. SIGNAL MODELS

Many theoretical models have been proposed to explain the MiniBooNE LEE. These include standard model backgrounds [7, 14–16], light sterile neutrinos (and variations) [17–19], heavy neutrino decay [20, 21], and dark-sector particles [22–24], amongst others. All models ultimately rely on assumptions about the interaction process that produces the observed excess events in the MiniBooNE detector. Yet, whichever model or interpretation is attributed to the LEE, it must ultimately be compatible with the kinematics of the LEE as observed in MiniBooNE.

In this note, we define *LEE Signal Model 1* as the same electron-like LEE model tested in Ref. [3]. This model is generated by unfolding the MiniBooNE excess according to the smearing matrix that describes the energy of charged-current quasi-elastic events as reconstructed by the MiniBooNE detector. However, this model suffers the limitation of not leading to shower kinematics consistent with those observed by MiniBooNE in the shower energy and shower angle variables, particularly for forward-going showers, as shown in Appendix C. This points to the overall challenge of finding a signal model that fully describes the MiniBooNE excess observation.

To overcome this limitation, this analysis uses both the electron shower energy and shower angle relative to the beam direction (θ) to expand the range of kinematic variables in which the ν_e interpretation of the MiniBooNE LEE is tested, in addition to the reconstructed neutrino energy. We construct a new signal model – labelled *LEE Signal Model 2* – by unfolding the background-subtracted excess of data events in the reconstructed shower energy and $\cos\theta$ two-dimensional space. This process utilizes MiniBooNE's selection efficiency of final-state electrons and the matrix that describes the smearing of reconstructed electron kinetic energy and angle. The ratio between this unfolded excess rate and the corresponding rate from MiniBooNE's intrinsic ν_e flux from the Booster Neutrino Beam (BNB) without an excess is used to obtain a scaling in each bin of shower energy and angle. This scaling is then applied to the true electron kinematics from MicroBooNE's intrinsic ν_e prediction to generate the predicted signal, leaving the modeling of the hadronic kinematics unchanged. More details detailing *LEE Signal Model 2* can be found in Appendix C.

V. RESULTS

The final distributions of data and MC simulation in the two signal channels are presented as a function of reconstructed neutrino energy in Fig. 2 for the $1e\mathrm{N}p0\pi$ selection and in Fig. 3 for the $1e0p0\pi$ selection with the relative prediction for the *LEE Signal Model 1*. Two noteworthy features observed in the previous analysis [3] were the small excess at very low energies observed in the $1e0p0\pi$ channel and and the deficit at medium energy in

the $1e\mathrm{N}p0\pi$ channel. The additional data included in this analysis does not exhibit an excess in the $1e0p0\pi$ channel, and does not show a statistically significant deficit in the medium energy region of the $1e\mathrm{N}p0\pi$ channel. Distributions for shower kinematics and the relative prediction for the *LEE Signal Model 2* are displayed in Figs. 4 - 7. Similarly to what was observed in [25], these show some over-prediction at intermediate electron energies and forward angles in the $1e\mathrm{N}p0\pi$ channel; the prediction and the observation match well in the $1e0p0\pi$ channel. Appendix E shows event displays of select $1e\mathrm{N}p0\pi$ and $1e0p0\pi$ candidates from data.

FIG. 2. Distribution of MC simulation compared with data for reconstructed neutrino energy in the $1e\mathrm{N}p0\pi$ signal channel, along with the *LEE Signal Model 1*.

Three statistical tests are performed on the data: a simple χ^2 test assuming H_0 (no excess), a $\Delta\chi^2$ test comparing H_0 to H_1 (no excess versus the full MiniBooNE signal), and finally a fit for the strength of the MiniBooNE signal. In every statistical test, we calculate frequentist p-values using pseudo-data trials. For each trial, we first sample a histogram of expectation values from a multivariate normal distribution according to the covariance matrix of systematic uncertainties, and then draw the pseudo-data from Poisson distributions with these expectation values. In this way, we accurately account for the effects of Poisson statistics. The tests are performed separately on the neutrino energy, shower energy, and shower $\cos\theta$ distributions. In case of the neutrino energy distribution, shown in Figs. 2 and 3, the histogram for the LEE hypothesis is calculated using the signal that has been unfolded using a smearing matrix constructed to model the effect of MiniBooNE's energy reconstruction. This calculation is described in more detail in Section IIID of Ref. [3]. The use of the same binning and signal model makes the results from this channel directly comparable to Ref. [3]. For *LEE Signal Model 2*, described in
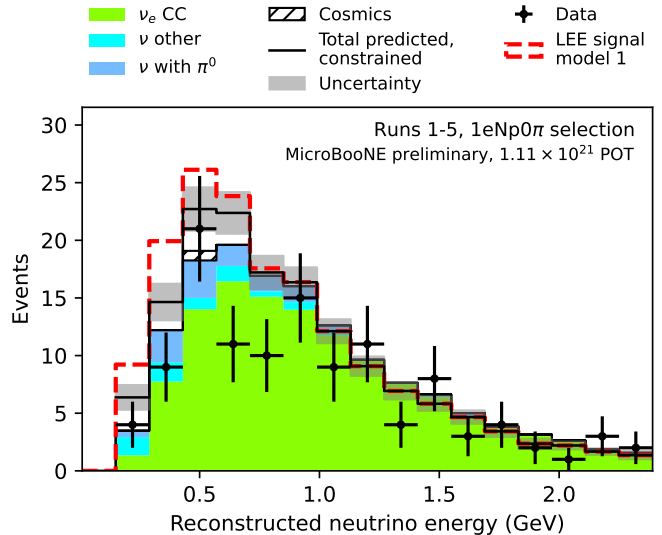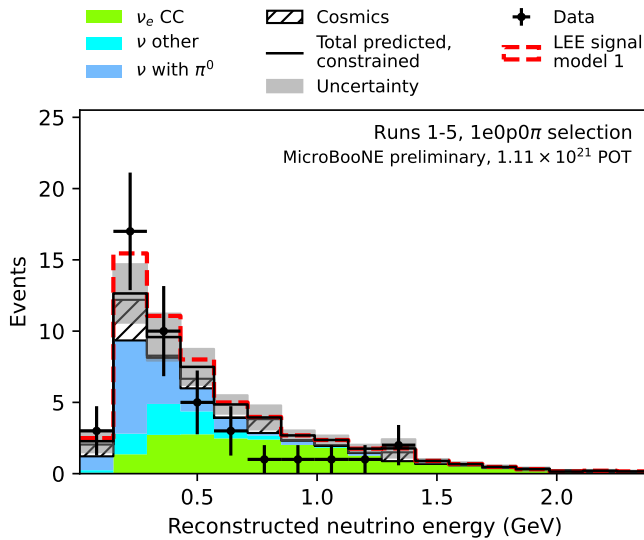
FIG. 3. Distribution of MC simulation compared with data for reconstructed neutrino energy in the $1e0p0\pi$ signal channel, along with the *LEE Signal Model 1*.
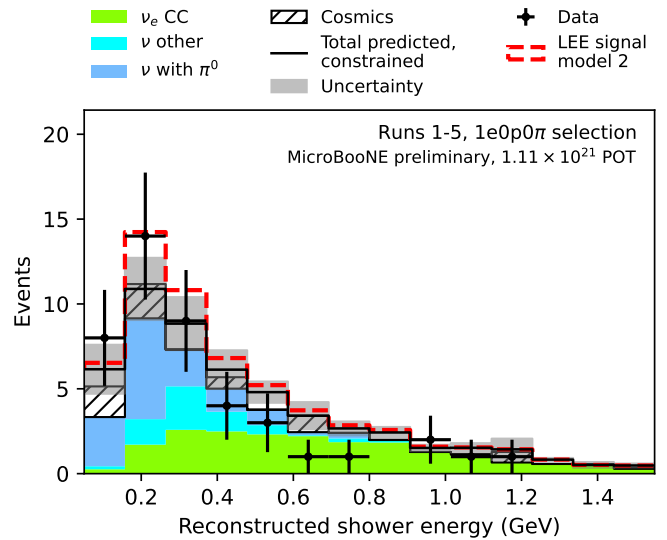

FIG. 5. Distribution of MC simulation compared with data for reconstructed shower energy in the $1e0p0\pi$ signal channel, along with the *LEE Signal Model 2*.
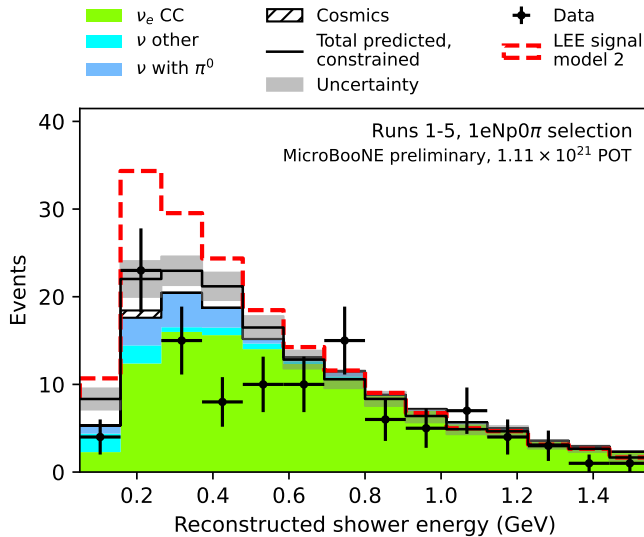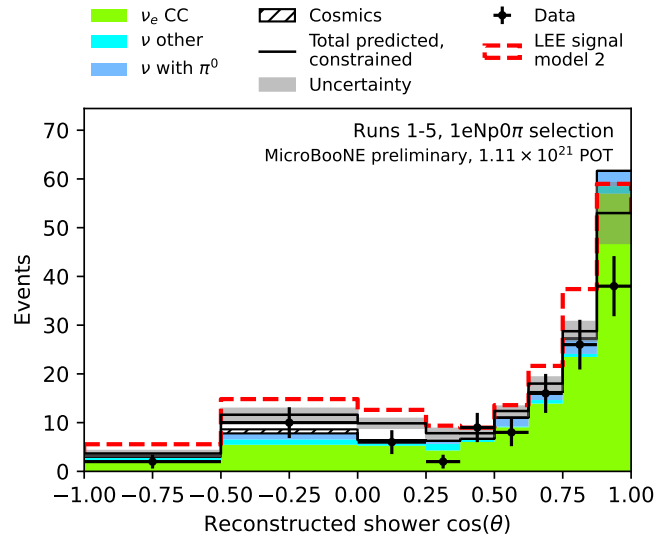

FIG. 4. Distribution of MC simulation compared with data for reconstructed shower energy in the $1e\mathrm{N}p0\pi$ signal channel, along with the *LEE Signal Model 2*.

FIG. 6. Distribution of MC simulation compared with data for reconstructed shower $\cos\theta$ in the $1e\mathrm{N}p0\pi$ signal channel, along with the *LEE Signal Model 2*.

Sec. IV, we perform the statistical tests independently in the shower energy and shower angle variables. The outcomes of all statistical tests are summarized in Table I.

We generally observe a good agreement between data and H_0, with frequentist p-values of 31.3%, 26.0%, and 43.4% for the null hypothesis for the combined signal channels in the neutrino energy, shower energy, and shower $\cos\theta$ distributions, respectively. When looking at the separate channels, p-values are $> 50\%$ in the $1e0p0\pi$ channel and $>10\%$ in the $1e\mathrm{N}p0\pi$ channel. For the channel with visible protons, this indicates that these distributions are compatible with the prediction after constraint

at the 1.6σ level.

In the two-hypothesis test, we reject the *LEE Signal Model 1* at 3.2σ CL and the *LEE Signal Model 2* at $> 4\sigma$. However, the observed $\Delta\chi^2$ test statistic is also in tension with the null hypothesis, particularly in the shower angle distribution which is the variable providing the strongest exclusion limits. In such a situation where the data contains fewer events than the background-only prediction, the signal exclusion could potentially be unreasonably strong. In order to calculate a more conservative confidence level, the modified frequentist CL_s method has been proposed in [26, 27]. Using this approach, we re-
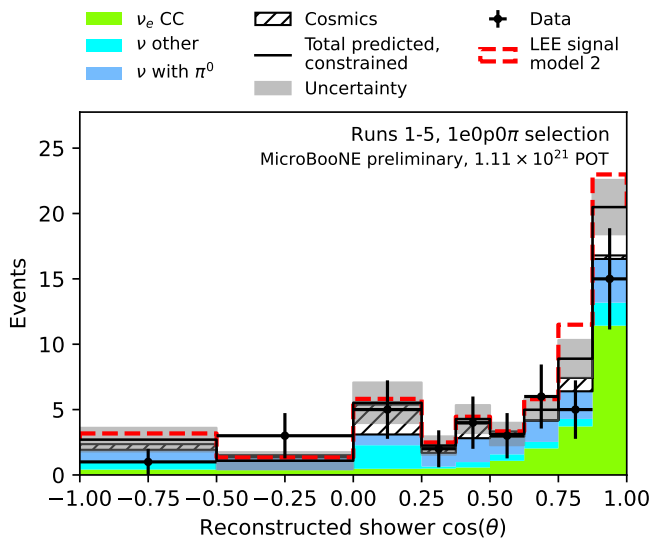
FIG. 7. Distribution of MC simulation compared with data for reconstructed shower $\cos\theta$ in the $1e0p0\pi$ signal channel, along with the *LEE Signal Model 2*.

ject the *LEE Signal Model 1* at 2.5σ and the *LEE Signal Model 2* at 3.5σ and 3.8σ when measured in the electron energy or electron angle, respectively. Further details on the two-hypothesis tests performed are provided in Appendix D.
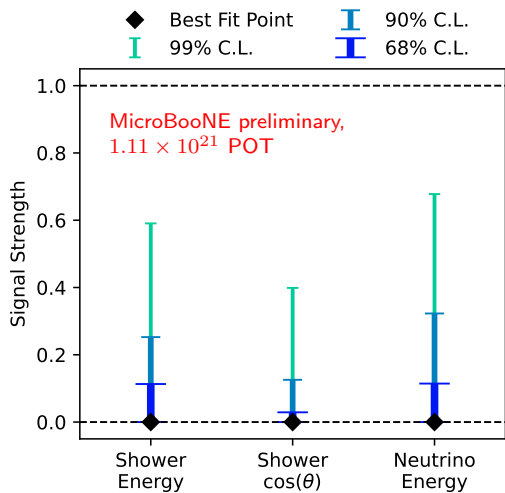

FIG. 8. Confidence intervals obtained for the fit to each variable using the combined $1e\mathrm{N}p0\pi$ and $1e0p0\pi$ channels. Confidence intervals shown are generated with the Feldman-Cousins procedure [28].

The result of the signal strength fits for all measured variables in the combined $1e\mathrm{N}p0\pi$ and $1e0p0\pi$ chan-

nels are shown in Fig. 8. In agreement with the two-hypothesis tests, the LEE hypothesis (that is, a signal strength of 1.0) is excluded at $> 99\%$ confidence level for every measured distribution when both signal channels are included. We also ran the fit separately for each measured channel, the results of which are shown in Fig. 9. The two-hypothesis tests and the signal strength fits for measurements using only the $1e0p0\pi$ signal channel show a weaker preference for H_0 over H_1. This demonstrates that the strong exclusion of the LEE hypothesis in the combined fit is mostly driven by the data in the $1e\mathrm{N}p0\pi$ channel.
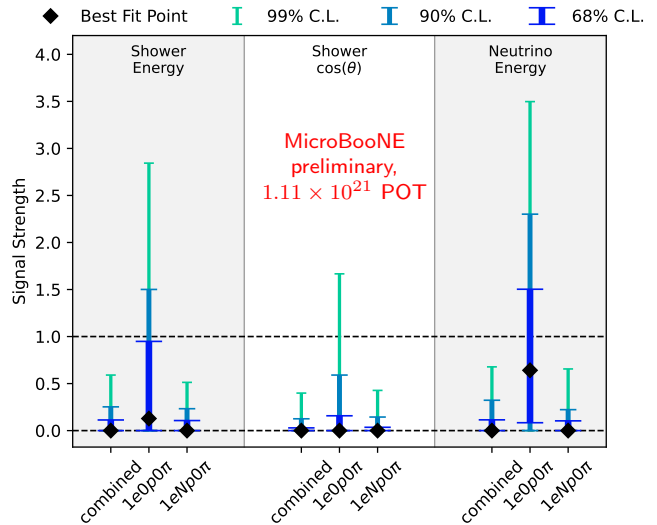

FIG. 9. Confidence intervals obtained from all fits performed in this analysis. Confidence intervals shown are generated with the Feldman-Cousins procedure [28].

VI. SUMMARY

This note presents an updated investigation of low energy electron-like events from the Booster Neutrino Beamline using the full MicroBooNE dataset $(1.1 \times 10^{21}$ POT). The analysis builds on earlier measurements which test the hypothesis that an anomalous excess is due to an energy-dependent scaling of the intrinsic electron neutrino rate, and complements this with new tests motivated by the observable kinematics (shower angle and energy) observed by MiniBooNE. In all kinematic variables, we find that our data is consistent with no excess of electron neutrino interactions, and excludes the ν_e interpretation of the MiniBooNE LEE at $\geq 99\%$ CL. While the MiniBooNE excess remains unexplained, after looking at additional data and kinematic variables, our measurements confirm our previous results and are inconsistent with a ν_e interpretation of the excess.

TABLE I. Summary of results with data corresponding to 1.11×10^{21} POT. The first three rows show the χ^2 between the data and the null hypothesis after constraint (H_0) and its corresponding p-value. Rows 4 through 8 show the results of the two-hypothesis test in which H_0 is compared to the signal model hypotheses (H_1). The median sensitivity gives the confidence level at which we would be able to reject the null hypothesis at the median $\Delta\chi^2$ expected under H_1. Finally, the confidence level for the H_1 hypothesis using the CL_s method is reported. The last three rows show the best fit point of the fitted signal strength, μ_{BF}, its upper limit at 2σ CL and the expected upper limit for the case that the data corresponded exactly to the prediction at H_0.

Signal Model	Signal Model 1			Signal Model 2						
Variable	Neutrino Energy			Electron Energy			Electron $\cos(\theta)$			
Channel	$1e\mathrm{N}p0\pi$	$1e0p0\pi$	Combined	$1e\mathrm{N}p0\pi$	$1e0p0\pi$	Combined	$1e\mathrm{N}p0\pi$	$1e0p0\pi$	Combined	Row
observed χ^2	15.0	9.9	24.9	23.3	13.3	35.9	14.4	6.2	19.8	1
ndof	10	10	20	14	14	28	9	9	18	2
$P(\chi^2>\mathrm{obs.}|H_0)$ [%]	18.4	56.1	31.3	10.4	62.5	26.0	15.3	77.6	43.4	3
obs. $H_0 - H_1\ \Delta\chi^2$	-11.3	0.4	-10.3	-15.3	-1.2	-15.2	-17.4	-4.6	-20.5	4
$P(\Delta\chi^2<\mathrm{obs.}|H_0)$ [%]	5.5	78.9	16.3	9.5	59.3	16.9	1.9	12.0	1.25	5
$P(\Delta\chi^2<\mathrm{obs.}|H_1)$ [%]	0.04	34.2	0.07	0.002	13.8	0.003	0.001	0.8	0.0001	6
Median sensitivity [%]	1.21	11.1	0.57	0.06	8.7	0.03	0.47	8.6	0.20	7
CL_s [%]	0.65	43	0.45	0.023	23	0.02	0.07	6.7	0.008	8
μ_{BF}	0.0	0.6	0.0	0.0	0.14	0.0	0.0	0.0	0.0	9
2σ CL upper limit on μ	0.34	2.64	0.47	0.34	1.90	0.39	0.24	0.88	0.22	10
Exp. 2σ CL limit	1.03	1.88	0.88	0.71	1.80	0.64	0.84	1.80	0.74	11

Appendix A: Demonstration of the CRT Impact on the Selection

To illustrate the impact of the CRT-based cuts, we show in Fig. 10 the prediction for the reconstructed neutrino energy distribution from the $1e0p0\pi$ selection after loose selection cuts have been applied without (left) and with (right) background rejection from the CRT. The CRT is responsible for "vetoing" events with any activity in-time with the neutrino interactions that trigger activity in the CRT panels surrounding the MicroBooNE cryostat. This cut is able to remove 60% of cosmic backgrounds, while rejecting only 3% of charged-current ν_e interactions. The MicroBooNE CRT system is described in Ref. [10].
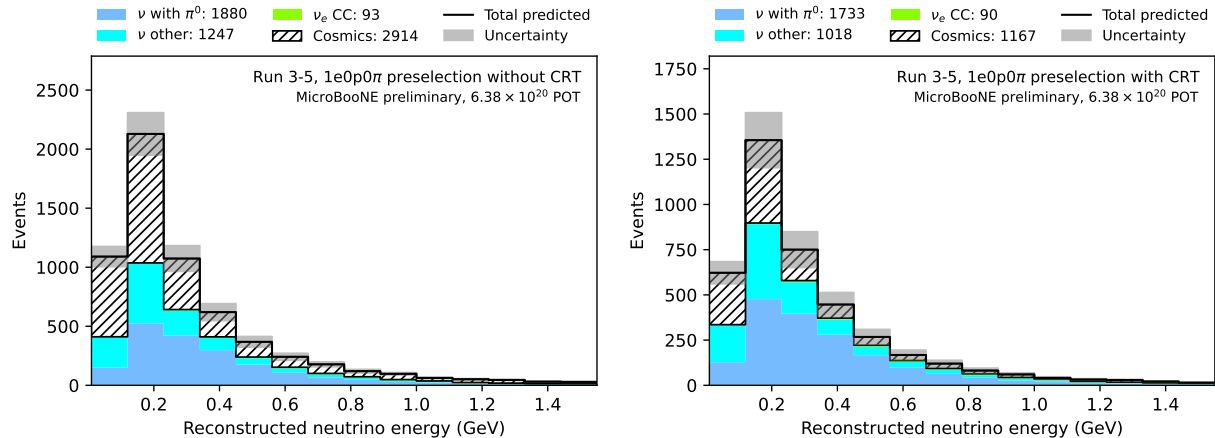
FIG. 10. Comparison of the predicted reconstructed neutrino energy distribution for the $1e0p0\pi$ preselection, with and without the application of CRT cuts to the event selection.

Appendix B: Constraint Covariance and Impact

This analysis leverages several sidebands to constrain both intrinsic ν_e and NC π^0 interactions (the leading source of background). The constraint is performed through the conditional constraint formalism, in the same way as in the first round of the analysis [3]. This constraint procedure relies on the correlations with sideband channels to update the prediction and its uncertainty in the signal region. As a demonstration of the information leveraged by the constraint and the impact it has on the analysis, we show in Fig. 11 the correlation matrix between signal channels (bottom left 2×2 quadrant) with sideband channels (top right 3×3 quadrant). Figure 12 then shows the impact the constraint has on the signal prediction for $1eNp0\pi$ (left) and $1e0p0\pi$ (right). In this figure the blue solid line and shaded region represents the predicted number of events and 1σ uncertainty before the constraint was produced. The analogous information in orange instead shows the constrained prediction and uncertainty. Informed by the data in the sidebands shown in Fig. 1, the CV slightly shifts in both distributions, and uncertainties generally shrink. The reduction in systematic uncertainty is greater in the $1eNp0\pi$ channel compared to the $1e0p0\pi$ channel.
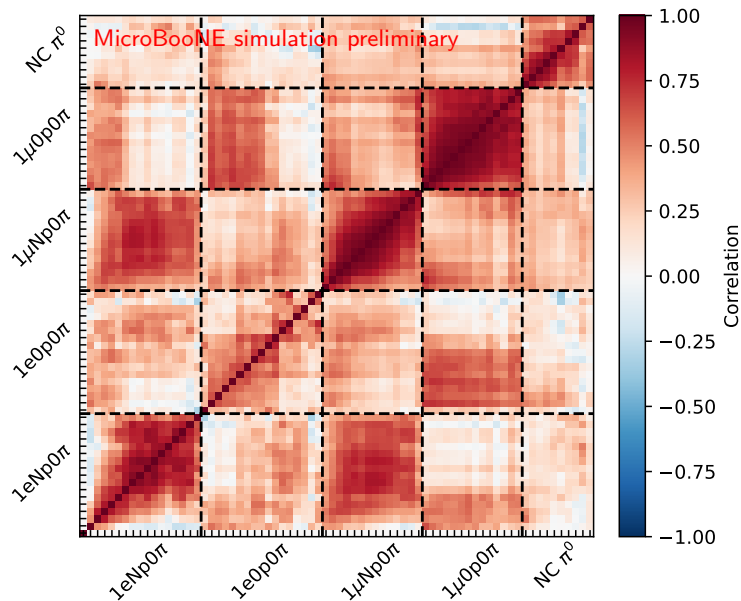
FIG. 11. Correlation matrix between the signal and sideband channels of the analysis. All channels are binned in reconstructed neutrino energy.
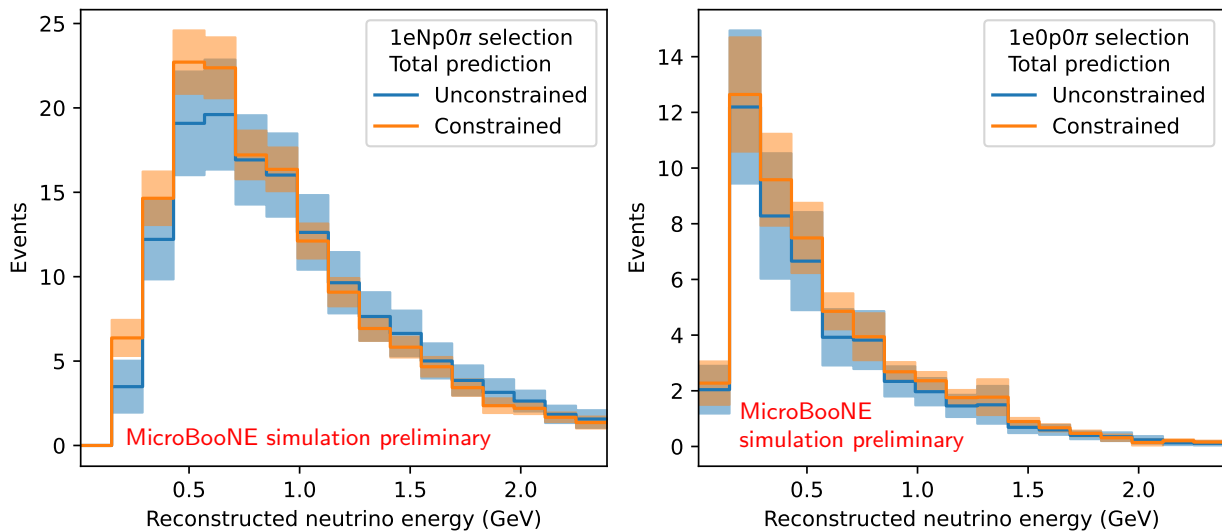

FIG. 12. Predictions in the $1eNp0\pi$ and $1e0p0\pi$ signal channels with uncertainties, before and after applying the constraint procedure.

Appendix C: Updated Signal Model

This appendix presents details tied to *LEE Signal Model 2* built in shower kinematics used in the analysis. While briefly described here, we note that the method by which the signal model is constructed follows the same prescription as documented in Ref. [29] to construct a neutrino-energy-based signal model (*LEE Signal Model 1*) and used for the first round of the analysis, though now with updated kinematic variables. The shower-kinematics-based signal model relies on MiniBooNE's efficiency and smearing matrix in shower energy and angle. The smearing matrices for shower energy and angle are shown in Fig. 13. Given the nature of these variables, and the uniform angular efficiency and resolution of the MiniBooNE detector, both smearing matrices show strong correlation between truth and reconstructed quantities. The efficiency for MiniBooNE to reconstruct electrons is roughly flat in these variables, averaging at 6.1%. While here we present the smearing matrices in one dimension to convey the true to reconstructed smearing of each variable, the full two-dimensional efficiency and smearing matrix is used in the unfolding.

The ratio between MiniBooNE's unfolded excess events and the electron kinematics of its intrinsic electron neutrino events is used to obtain a scaling of the electron neutrino events in each two-dimensional bin, as shown in Fig. 14. The enhanced rate of ν_e-induced electron events is particularly pronounced in the most forward-going and low-energy bin, with enhancement of more than ten times the intrinsic electron neutrino rate. Fig. 15 and Fig. 16 show MicroBooNE's truth-level electron energy and $\cos\theta$ spectra broken into final-state topology, without any selection cuts applied, for *LEE Signal Model 1* and *2*, respectively. The *LEE Signal Model 2* obtained from the MiniBooNE dataset predicts a visible excess primarily in the range of 150-500 MeV for electron energy, and 0.7-1.0 for electron $\cos\theta$.
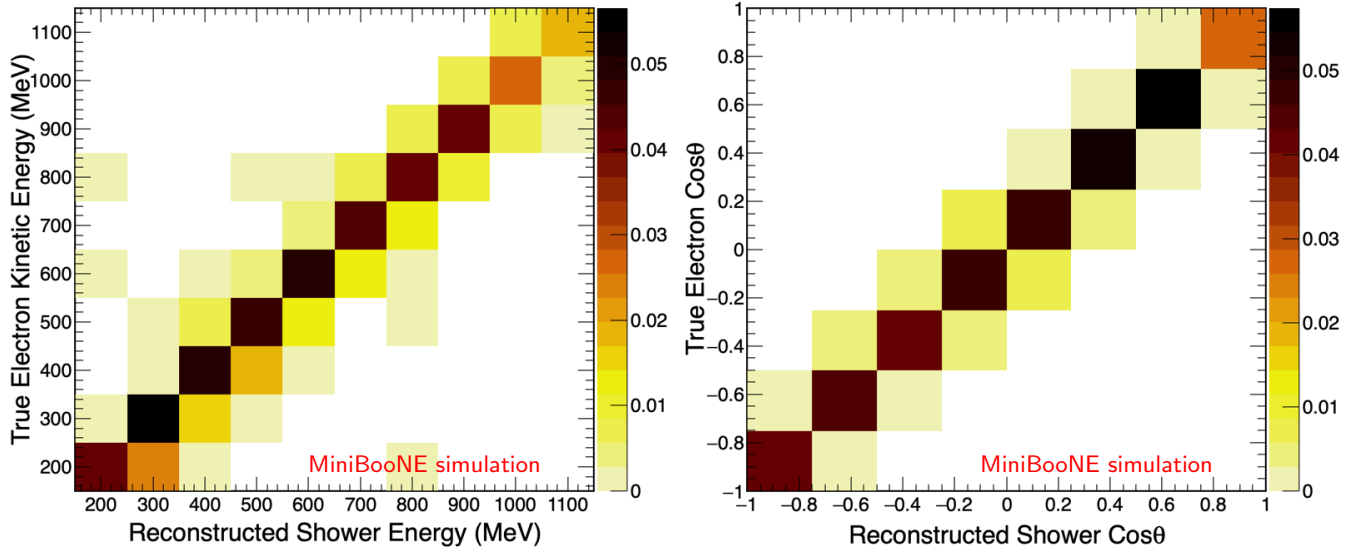
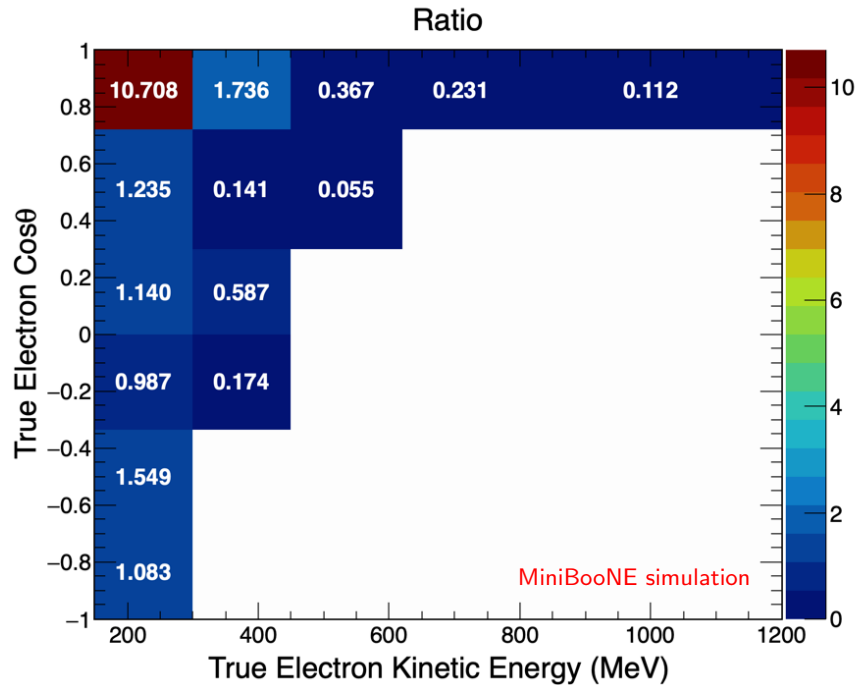FIG. 13. MiniBooNE response matrix for electron shower energy and $\cos(\theta)$.

FIG. 14. The LEE ratio model unfolded from MiniBooNE shower two-dimensional kinematic variables.
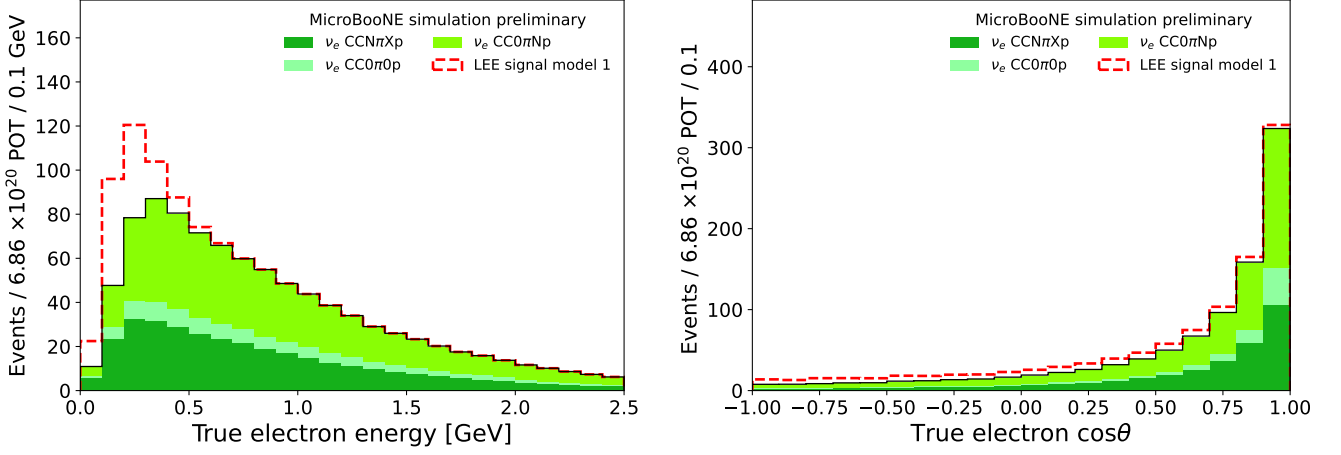
FIG. 15. The *LEE Signal Model 1* on MicroBooNE electron kinematics spectra in truth ν_e events before any selection cuts applied.
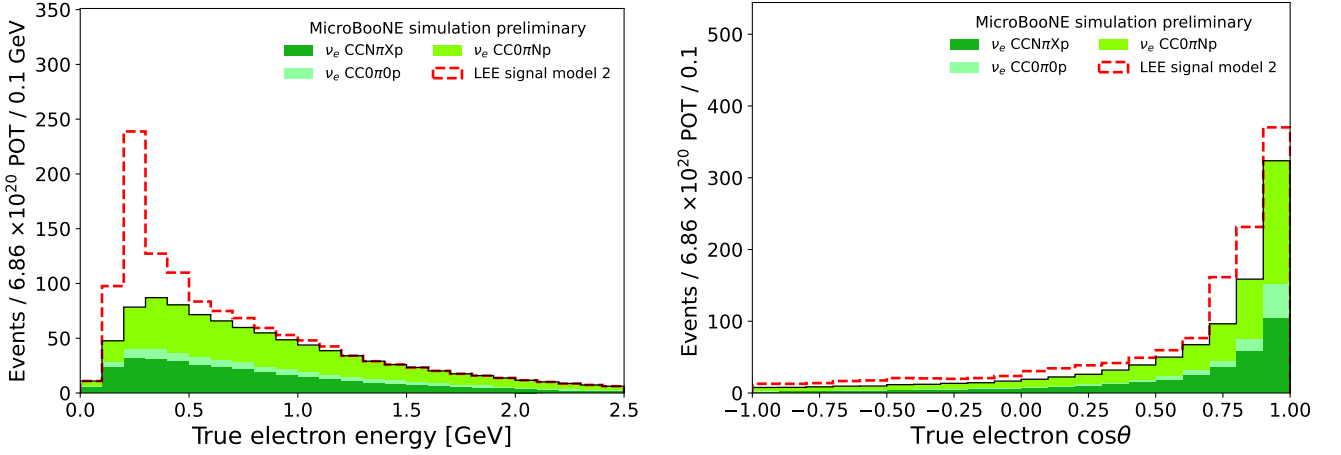

FIG. 16. The *LEE Signal Model 2* on MicroBooNE electron kinematics spectra in truth ν_e events before any selection cuts applied.

Appendix D: Two-Hypothesis Tests

This appendix shows the two-hypothesis test results performed in the analysis. Several tests are performed to test both *LEE Signal Model 1* (based on unfolded neutrino energy, the same model used in the first iteration of this analysis [3]) as well as *LEE Signal Model 2* (built from the underlying shower kinematics). The tests are further repeated for the $1eNp0\pi$ and $1e0p0\pi$ channels separate and combined. In each figure two curves are shown, representing the distribution of $\Delta\chi^2$ values obtained from toy experiments under the assumption that the null-hypothesis (no signal, H_0, in blue) is the underlying truth or that the signal model (H_1, in orange) represents the underlying truth. The vertical dashed line represents the median result for H_1 and is used to calculate the median sensitivity for ruling out the signal model hypothesis if the H_0 hypothesis were true. The vertical solid line represents the observed $\Delta\chi^2$.

Figure 17 shows two-hypothesis test results for the test of *LEE Signal Model 2* in the combined $1eNp0\pi$ and $1e0p0\pi$ channels. The fit is performed in shower energy (left) and shower $\cos\theta$ (right). Figure 18 shows expectations and results for a test of model 2 but now for the $1eNp0\pi$ alone. Figure 19 shows expectations and results for a test of model 2 but now for the $1e0p0\pi$ alone. Figure 20 shows expectations and results for a test of model 1 for the two channels combined. Tests for model 1 for $1eNp0\pi$ and $1e0p0\pi$ separately are shown in Fig. 21 in the left and right panels, respectively.
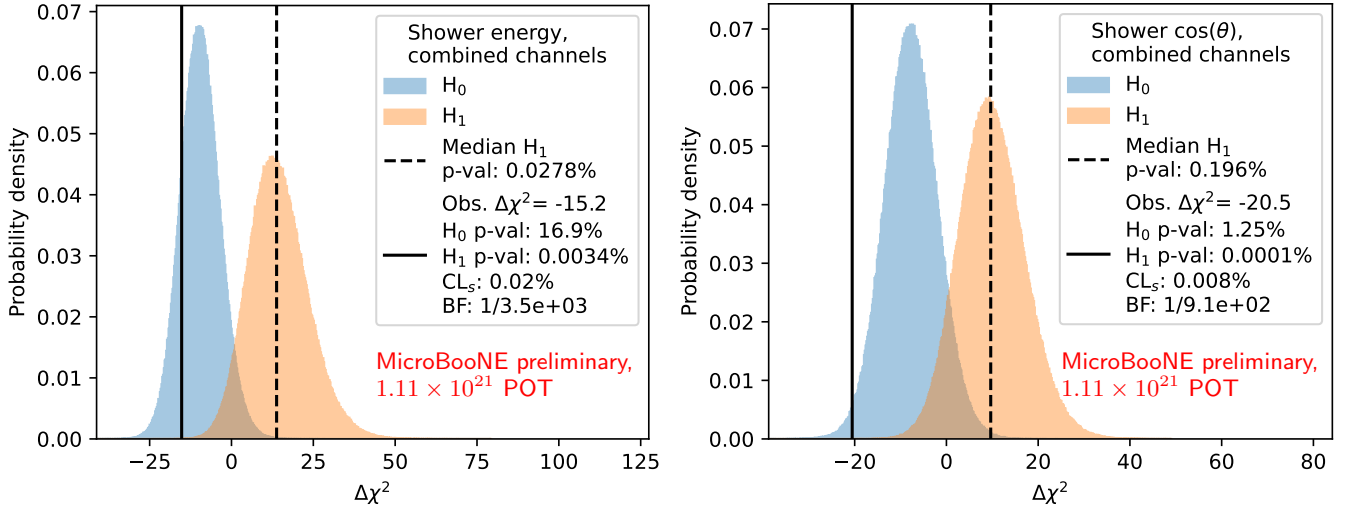
FIG. 17. Two-hypothesis test using the *LEE Signal Model 2* based on shower kinematics binned in shower energy (left) and angle (right), for the combined $1e\mathrm{N}p0\pi$ and $1e0p0\pi$ channels. The Bayes Factor (BF) is the probability density of the observed $\Delta\chi^2$ under H_1 divided by the probability density under H_0.
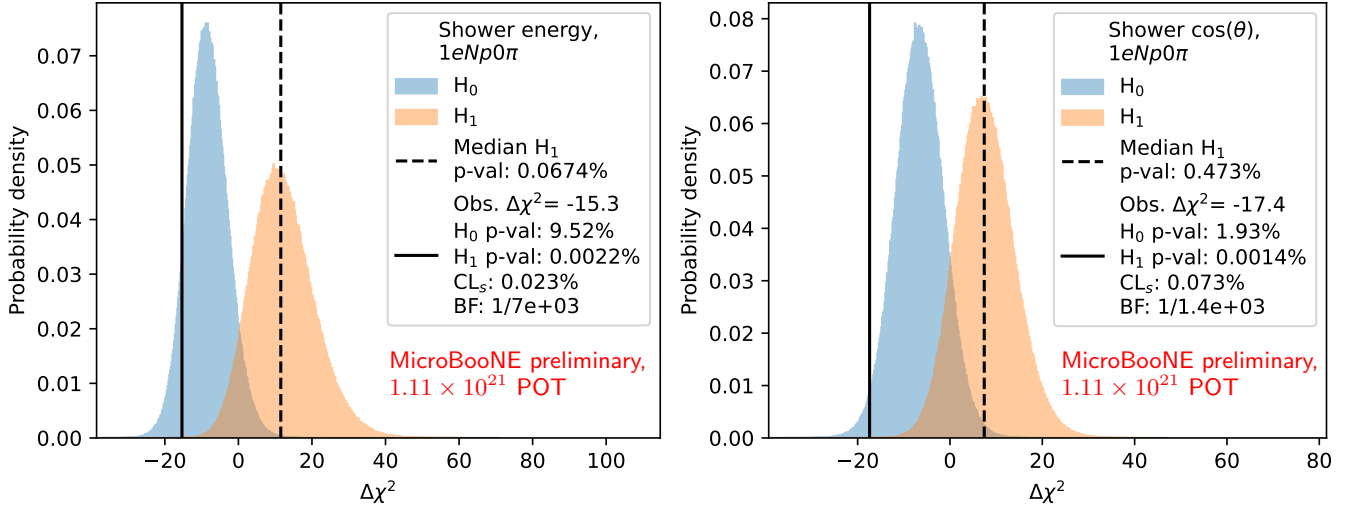

FIG. 18. Two-hypothesis test using the *LEE Signal Model 2*, binned in shower kinematics (left: shower energy, right: shower $\cos\theta$), for the individual $1e\mathrm{N}p0\pi$ channel.
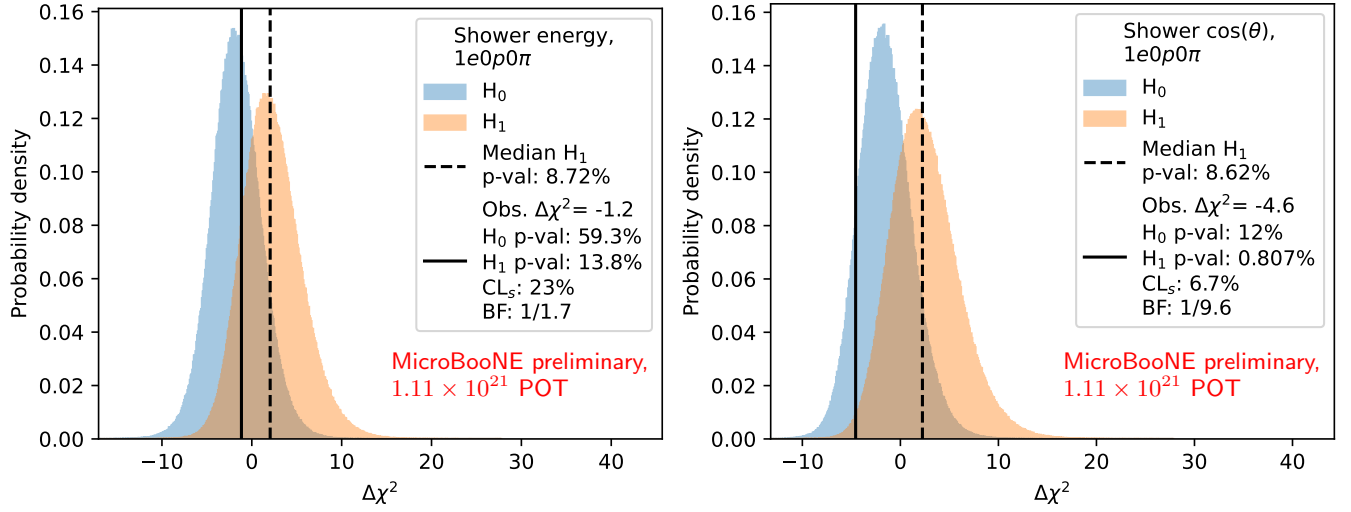
FIG. 19. Two-hypothesis test using the *LEE Signal Model 2*, binned in shower kinematics (left: shower energy, right: shower $\cos\theta$), for the individual $1e0p0\pi$ channel.
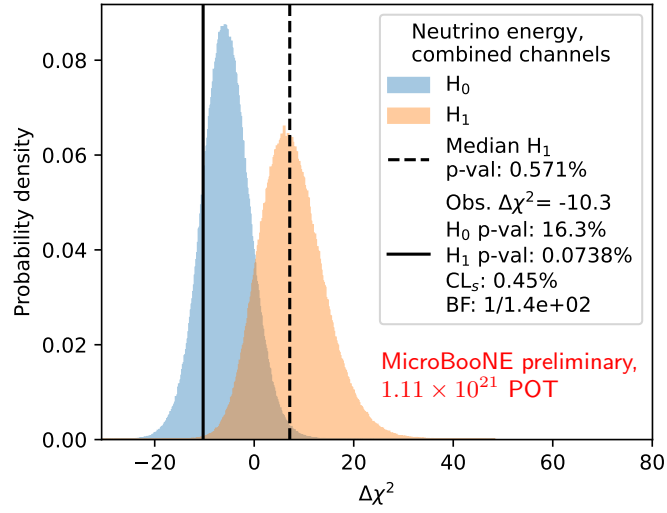

FIG. 20. Two-hypothesis test using the *LEE Signal Model 1*, binned in neutrino energy, for the combined $1eNp0\pi$ and $1e0p0\pi$ channels.
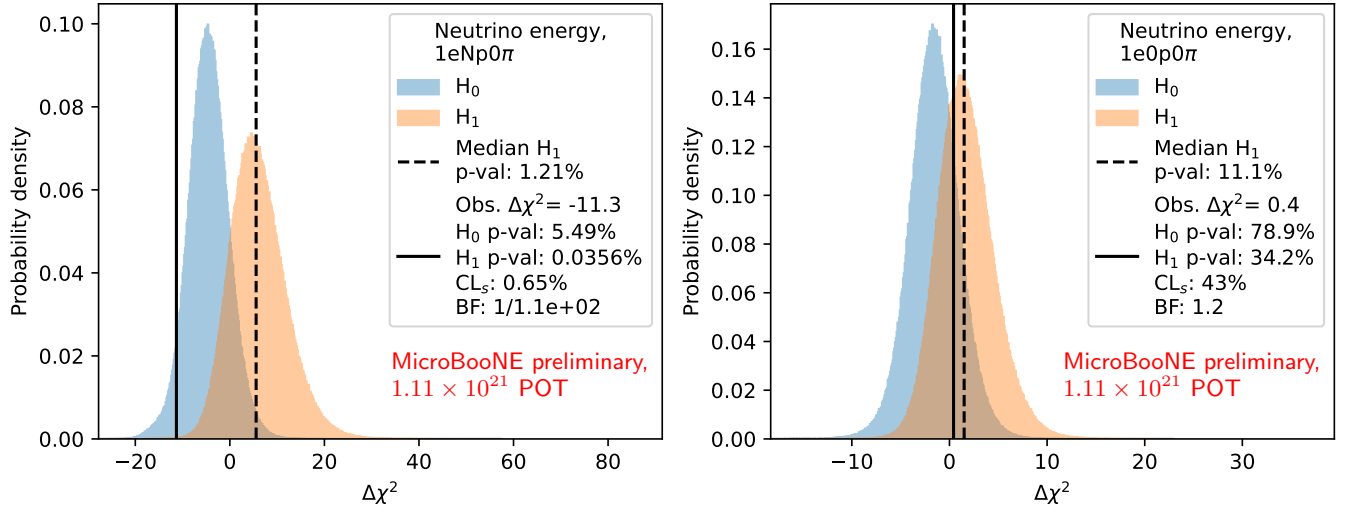
FIG. 21. Two-hypothesis test using the *LEE Signal Model 1*, binned in neutrino energy, for the individual signal channels (left: $1eNp0\pi$, right: $1e0p0\pi$).

Appendix E: Event Displays

This section shows event displays of selected candidate events from the $1e0p0\pi$ (Fig 22) and $1e\mathrm{N}p0\pi$ (Fig. 23) selections.
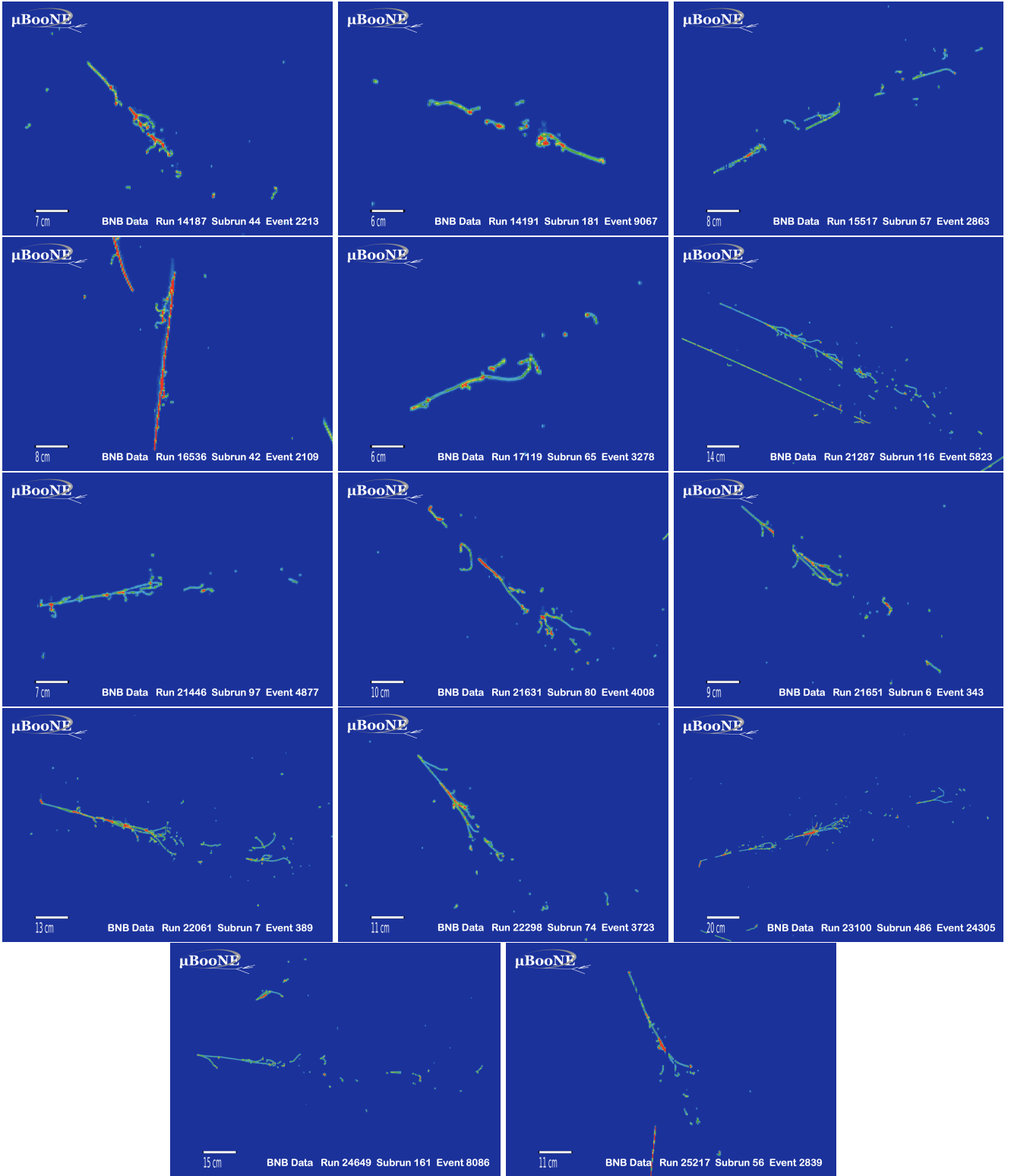

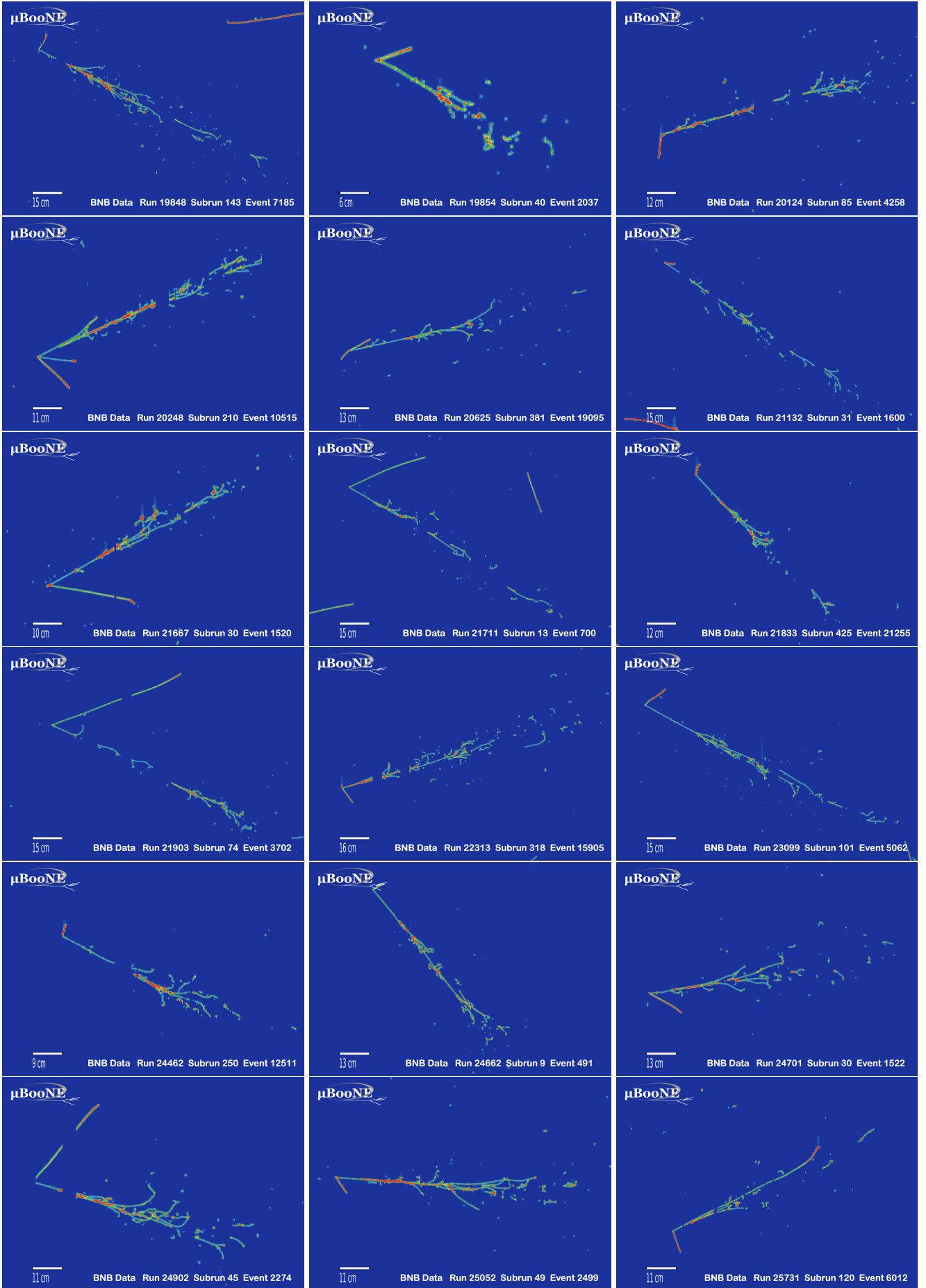FIG. 22. Event displays of selected electron neutrino candidate data events in the $1e0p0\pi$ signal channel.

FIG. 23. Event displays of selected electron neutrino candidate data events in the $1e\mathrm{N}p0\pi$ signal channel.

[1] R. Acciarri *et al.* (MicroBooNE Collaboration), Design and Construction of the MicroBooNE Detector, JINST **12** (02), P02017.

[2] A. A. Aguilar-Arevalo *et al.* (MiniBooNE Collaboration), Significant excess of electronlike events in the miniboone short-baseline neutrino experiment, Phys. Rev. Lett. **121**, 221801 (2018).

[3] P. Abratenko *et al.* (MicroBooNE Collaboration), Search for an anomalous excess of charged-current ν_e interactions without pions in the final state with the microboone experiment, Phys. Rev. D **105**, 112004 (2022).

[4] P. Abratenko *et al.* (MicroBooNE Collaboration), Search for an Excess of Electron Neutrino Interactions in MicroBooNE Using Multiple Final-State Topologies, Phys. Rev. Lett. **128**, 241801 (2022).

[5] P. Abratenko *et al.* (MicroBooNE Collaboration), Search for an anomalous excess of charged-current quasielastic νe interactions with the MicroBooNE experiment using Deep-Learning-based reconstruction, Phys. Rev. D **105**, 112003 (2022).

[6] P. Abratenko *et al.* (MicroBooNE Collaboration), Search for an anomalous excess of inclusive charged-current ν_e interactions in the MicroBooNE experiment using Wire-Cell reconstruction, Phys. Rev. D **105**, 112005 (2022).

[7] P. Abratenko *et al.* (MicroBooNE Collaboration), Search for Neutrino-Induced Neutral-Current Δ Radiative Decay in MicroBooNE and a First Test of the MiniBooNE Low Energy Excess under a Single-Photon Hypothesis, Phys. Rev. Lett. **128**, 111801 (2022).

[8] P. Abratenko *et al.* (MicroBooNE Collaboration), New $CC0\pi$ GENIE model tune for MicroBooNE, Phys. Rev. D **105**, 072001 (2022).

[9] R. Acciarri *et al.* (MicroBooNE Collaboration), The Pandora multi-algorithm approach to automated pattern recognition of cosmic-ray muon and neutrino events in the MicroBooNE detector, Eur. Phys. J. C **78**, 82 (2018).

[10] C. Adams *et al.* (MicroBooNE Collaboration), Design and construction of the MicroBooNE Cosmic Ray Tagger system, JINST **14** (04), P04004.

[11] P. Abratenko *et al.* (MicroBooNE Collaboration), Novel approach for evaluating detector-related uncertainties in a LArTPC using MicroBooNE data, Eur. Phys. J. C **82**, 454 (2022).

[12] X. Ji, W. Gu, X. Qian, H. Wei, and C. Zhang, Combined Neyman–Pearson chi-square: An improved approximation to the Poisson-likelihood chi-square, Nucl. Instrum. Meth. A **961**, 163677 (2020).

[13] M. L. Eaton, *Multivariate statistics*, Probability & Mathematical Statistics S. (John Wiley & Sons, Nashville, TN, 1983).

[14] A. A. Aguilar-Arevalo *et al.* (MiniBooNE), Updated MiniBooNE neutrino oscillation results with increased data and new background studies, Phys. Rev. D **103**, 052002 (2021).

[15] K. J. Kelly and J. Kopp, More ingredients for an Altarelli cocktail at MiniBooNE, JHEP **05**, 113.

[16] V. Brdar and J. Kopp, Can standard model and experimental uncertainties resolve the miniboone anomaly?, Physical Review D **105**, 10.1103/physrevd.105.115024 (2022).

[17] A. Diaz, C. Argüelles, G. Collin, J. Conrad, and M. Shaevitz, Where are we with light sterile neutrinos?, Physics Reports **884**, 1 (2020).

[18] S. Böser, C. Buck, C. Giunti, J. Lesgourgues, L. Ludhova, S. Mertens, A. Schukraft, and M. Wurm, Status of light sterile neutrino searches, Progress in Particle and Nuclear Physics **111**, 103736 (2020).

[19] S. Vergani, N. W. Kamp, A. Diaz, C. A. Argüelles, J. M. Conrad, M. H. Shaevitz, and M. A. Uchida, Explaining the MiniBooNE excess through a mixed model of neutrino oscillation and decay, Phys. Rev. D **104**, 095005 (2021).

[20] L. Alvarez-Ruso and E. Saul-Sala, Radiative decay of heavy neutrinos at MiniBooNE and MicroBooNE, in *Prospects in Neutrino Physics* (2017) arXiv:1705.00353 [hep-ph].

[21] O. Fischer, A. Hernández-Cabezudo, and T. Schwetz, Explaining the MiniBooNE excess by a decaying sterile neutrino with mass in the 250 MeV range, Phys. Rev. D **101**, 075045 (2020).

[22] A. Abdullahi, M. Hostert, and S. Pascoli, A dark seesaw solution to low energy anomalies: MiniBooNE, the muon (g−2), and BaBar, Phys. Lett. B **820**, 136531 (2021).

[23] E. Bertuzzo, S. Jana, P. A. N. Machado, and R. Zukanovich Funchal, Dark Neutrino Portal to Explain MiniBooNE excess, Phys. Rev. Lett. **121**, 241801 (2018).

[24] P. Ballett, S. Pascoli, and M. Ross-Lonergan, U(1)' mediated decays of heavy sterile neutrinos in MiniBooNE, Phys. Rev. D **99**, 071701 (2019).

[25] P. Abratenko *et al.* (MicroBooNE Collaboration), Differential cross section measurement of charged current νe interactions without final-state pions in MicroBooNE, Phys. Rev. D **106**, L051102 (2022).

[26] T. Junk, Confidence level computation for combining searches with small statistics, Nuclear Instruments and Methods in Physics Research Section A: Accelerators, Spectrometers, Detectors and Associated Equipment **434**, 435 (1999).

[27] A. L. Read, Modified frequentist analysis of search results (the cl(s) method) (2000).

[28] G. J. Feldman and R. D. Cousins, Unified approach to the classical statistical analysis of small signals, Phys. Rev. D **57**, 3873 (1998).

[29] MicroBooNE Collaboration, Low-energy excess signal prediction from unfolding MiniBooNE Monte-Carlo and data, MICROBOONE-NOTE-1043-PUB, DOI:10.2172/1573217 (2018).